Dynamic Contrast-Enhanced Magnetic Resonance Imaging Rapidly Indicates Vessel Regression in Human Squamous Cell Carcinomas Grown in Nude Mice Caused by VEGF Receptor 2 Blockade with DC101[1]

Fabian Kiessling, Nabeel Farhan*, Matthias P. Lichy†, Silvia Vosseler‡, Melanie Heilmann*, Martin Krix†, Peter Bohlen§, Dan W. Miller¶, Margareta M. Mueller‡, Wolfhard Semmler*, Norbert E. Fusenig‡ and Stefan Delorme†*

Divisions of *Medical Physics in Radiology, †Radiology and ‡Carcinogenesis and Differentiation, German Cancer Research Center, INF 280, Heidelberg 96121, Germany; §ImClone Systems, Incorporated, 180 Varick Street, New York, NY 10014, USA; ¶Department of Ophthalmology, University Heidelberg, INF 400, Heidelberg 69120, Germany

Abstract

The purpose of our study was the investigation of early changes in tumor vascularization during antiangiogenic therapy with the vascular endothelial growth factor (VEGF) receptor 2 antibody (DC101) using dynamic contrast-enhanced magnetic resonance imaging (DCE MRI). Subcutaneous heterotransplants of human skin squamous cell carcinomas in nude mice were treated with DC101. Animals were examined before and repeatedly during 2 weeks of antiangiogenic treatment using Gd-DTPA–enhanced dynamic T1-weighted MRI. With a two-compartment model, dynamic data were parameterized in ''amplitude'' (increase of signal intensity relative to precontrast value) and k_{ep} (exchange rate constant). Data obtained by MRI were validated by parallel examinations of histological sections immunostained for blood vessels (CD31). Already 2 days after the first DC101 application, a decrease of tumor vascularization was observed, which preceded a reduction of tumor volume. The difference between treated tumors and controls became prominent after 4 days, when amplitudes of treated tumors were decreased by 61% (P = .02). In line with change of microvessel density, the decrease in amplitudes was most pronounced in tumor centers. On day 7, the mean tumor volumes of treated (153 ± 843 mm^3) and control animals (596 ± 384 mm^3) were significantly different (P = .03). After 14 days, treated tumors showed further growth reduction (83 ± 93 mm^3), whereas untreated tumors (1208 ± 822 mm^3) continued to increase (P = .02). Our data underline the efficacy of DC101 as antiangiogenic treatment in human squamous cell carcinoma xenografts in nude mice and indicate DCE MRI as a valuable tool for early detection of treatment effects before changes in tumor volume become apparent.

Neoplasia (2004) **6**, 213–223

Keywords: Angiogenesis, tumor, DCE MRI, DC101, VEGF.

Introduction

Angiogenesis is an essential step for the growth and spread of malignant tumors [1–3]. As a consequence, heightened interest has been placed on the mechanisms controlling this process and the identification of antiangiogenic targets [4,5]. Angiogenic inhibitors have been developed and successfully applied in syngenic and heterotransplant tumor models [6–8] and some of these drugs already entered phase I clinical trials [4,9–11]. Many of these inhibitors are directed against the vascular endothelial growth factor (VEGF) or its receptors, which are considered to play a key role in angiogenesis [6,12]. VEGF is both proangiogenic and antiapoptotic for endothelial cells, induces the development of immature blood vessels [13], and increases vessel permeability [14,15]. Inhibition of VEGF and its receptors stops the formation of new vessels in tumors, induces the regression of existing tumor vessels, and as a consequence leads to the collapse and necrotic degeneration of tumors [6,12].

Important for clinical application in antiangiogenic therapy is the early assessment of therapeutic effects for the prediction of therapy response and the individualization of treatment to impart confidence in drug development and dose finding [16,17]. Thus, functional monitoring of the effects of angiogenic inhibitors on tumor vasculature has become the focus of both basic and clinical research. Magnetic resonance imaging (MRI) provides several techniques for examining tissue vascularization and perfusion [18–22] that have already been successfully applied in patients for the characterization of tumors and

Abbreviations: DCE MRI, dynamic contrast-enhanced magnetic resonance imaging; Gd, gadolinium; TE, echo time; TR, repetition time; DTPA, diethylenetriaminepentaacetic acid; SCC, squamous cell carcinoma; DC101, inhibitory anti–VEGF receptor 2 antibody (ImClone Systems, Incorporated)

Address all correspondence to: Fabian Kiessling, MD, Division of Medical Physics in Radiology, German Cancer Research Center, Im Neuenheimer Feld 280, Heidelberg 69120, Germany. E-mail: f.kiessling@dkfz.de

[1]This work was supported by a grant from DFG, Schwerpunktprogramm Angiogenesis (FU91/5-1) (to N.E.F., S.V., and M.M.M.).

Received 12 October 2003; Revised 24 November 2003; Accepted 26 November 2003.

DOI 10.1593/neo.03394

monitoring of therapy response. In this regard, dynamic contrast-enhanced T1-weighted MRI, in combination with postprocessing of data using an open pharmacokinetic two-compartment model, has shown potential in clinical studies of the breast [23,24], cervix [25,26], and bone marrow [27].

However, the assessment of tissue perfusion in cancer still needs optimization. Dynamic parameters need to be validated in different tumor types with variable vascular architecture and reliable parameters for treatment monitoring have to be established. Furthermore, the ideal time point to start treatment monitoring using dynamic MR techniques has to be elucidated. For this purpose, in particular for monitoring during therapeutic intervention with antiangiogenic drugs, the use of small animals is required. Noninvasive dynamic MR studies of tumor angiogenesis in animals such as the mouse, however, are more difficult due to small animal and tumor volumes, and therefore usually need to be performed in dedicated animal MR scanners [20,28,29]. Although such studies give valuable information about tumor biology and also offer the opportunity to evaluate and improve new MR techniques or new contrast agents [30,31], their applicability is restricted due to the limited number of animal scanners available. We decided to perform our experiments on a clinical 1.5-T whole-body MR scanner using a self-developed small animal transmit-and-receive volume resonator, and were previously able to show that examination of mice can be done successfully and reliably with this setup [32]. Doing so, we expected that this setting would better match with clinical MR studies.

It was previously shown by histological analysis that the therapeutic VEGF receptor 2 antibody DC101 effectively inhibits tumor vascularization manifested in a marked decrease of tumor vessel density [33]. Concomitantly with this inhibition of angiogenesis, the antibody treatment also inhibited tumor invasion [33]. Although previous studies examined late effects of VEGF receptor 2 inhibition by histological methods (i.e., *ex vivo*), the purpose of our study was to monitor *in vivo* the early effects (3 hours–2 weeks) of this antibody treatment by dynamic T1-weighted contrast-enhanced MRI. For comparative validation of the MR results, histological specimens were obtained at the same time intervals as the MR measurements, from a second set of identically treated tumor-bearing animals.

Materials and Methods

Tumor Implantation and VEGF Receptor Antibody Treatment

All experiments were approved by the governmental review committee on animal care. Immortal human skin keratinocytes (HaCaT) tumorigenically transformed by Ha-ras transfection were selected for tumor progression by repeated *in vivo* passaging as nude mouse heterotransplants (HaCaT-ras-A-5RT3) [34,35]. Tumors were induced by subcutaneous injection of 2×10^5 cells, 0.5 to 1.0 cm behind the neck of nude mice. Starting at day 15 after tumor induction (mean tumor volume: 92 mm^3), mice were treated with a solution of 800 μg of VEGF receptor antibody (DC101; ImClone Systems, Incorporated, New York, NY) in 60 μl of NaCl, injected subcutaneously every other day [33]. In control animals, 60 μl of NaCl solution without DC101 was injected subcutaneously at identical time points. The effect of an irrelevant antibody control *versus* DC101 was examined previously [33] and found to have no effect. Intraperitoneal injection of antibody was evaluated as a second route of administration, and was found to yield the same results during the observation period (data not shown). The subcutaneous injection was given at a distance more than 1.5 cm from the tumor borders.

Examination Protocol

A total of 12 nude mice with subcutaneous squamous cell carcinomas (SCCs) was examined by MRI starting on day 15 after subcutaneous injection of tumor cells. Six were treated with the VEGF receptor antibody and six were kept as control animals. Six additional mice (control/therapy: $n = 3/3$) were carried as potential replacements (Table 1).

Six animals of the control and treatment groups were examined at each time point using MRI, with the exception of 1- and 3-hour time points (Table 1). At 1 and 3 hours, only three mice each of the therapy group were investigated because the contrast agent would not have been excreted by the organism within 3 hours.

The baseline MR examination was performed 1 day before starting treatment with the VEGF receptor antibody.

Table 1. Examination Protocol of the Study.

Mouse		Hours, days							
		0 hour	1 hour	3 hours	1 day	2 days	4 days	7 days	14 days
Follow-up group									
Treated	1	e	e		e	e	e	e, r	
	2	e	e		e	e	e	e	f, r
	3	e	e		e	e	e	e	e, r
	4	e		e	e	e	e	e	e, r
	5	e		e	e	e	e	e	e, r
	6	e		e	e	e	e	e	e, r
	R1-3								r
Untreated	7	e	e		e	f	e	e	e, r
	8	e	e		e	e	e	e	e, r
	9	e	e		e	e	e	e	e, r
	10	e		e	e	e	e	e	e, r
	11	e		e	e	e	e	e	e, r
	12	e		e	e	e	e	e	e, r
	R4-6								r
Correlation group									
Treated	1				e, r				
	2					e, r			
	3						e, r		
	4							e, r	
	5								e, r
Untreated	6				e, r				
	7					e, r			
	8						e, r		
	9							e, r	
	10								e, r

A group of 12 animals (six treated) was examined repeatedly using MRI. The correlation group was examined once by MRI and tumors were removed for histological evaluation after examination.
R, reserve group to replace dropouts; e, successful examination; f, examination failed; r, tumor removed for histology.

Follow-up examinations took place 1 hour (treated mice: $n = 3$), 3 hours (treated mice: $n = 3$), and 1, 2, 4, 7, and 14 days following the first anti–VEGF receptor antibody application. One treated and one control animal were sacrificed 7 days after the start of treatment for histological assessment. All other tumors were obtained after the final follow-up MR examination (i.e., 14 days after the start of VEGF receptor antibody treatments).

For histological comparisons with each of the time points of the MRI examination, a second study with 10 additional tumor-bearing animals was performed. At 1, 2, 4, and 7 days after start of the VEGF receptor antibody treatment, one treated and one control animal were examined with dynamic contrast-enhanced magnetic resonance imaging (DCE MRI) and sacrificed immediately after the examination.

Anesthesia and Application of Contrast Agent

For MR examination and catheterization, mice were anesthesized by inhalation of a mixture of isofluorane (1.5%), N_2O (35%), and O_2 (60%). A tail vein was catheterized using a 30-gauge needle connected to a 10-cm-long PE 10 polyethylene catheter (Portex, Medic-Eschmann, Germany) filled with 10 μl of 0.9% NaCl. Successful puncture of the mouse tail vein was controlled by blood reflux into the catheter and by injection of 30 μl of 0.9% NaCl. The needle was fixed on the mouse tail with superglue. The distal end of the catheter was connected with a 30-cm-long PE 50 polyethylene catheter (Portex) and a 1-ml tuberculin syringe, both containing the contrast agent. After each examination, the needle was removed from the tail vein.

Gadolinium diethylenetriaminepentaacetic acid (Gd-DTPA) (Magnevist Schering, Berlin, Germany) was diluted 1:5 in 0.9% NaCl. One hundred microliters of this solution (0.4 mmol/kg Gd-DTPA) was injected manually as a bolus within 5 seconds into the tail vein of nude mice.

MRI

MRI was performed on a clinical 1.5-T whole-body MRI system (Siemens Magnetom Vision, Erlangen, Germany) using a custom-made radiofrequency (rf) coil ("animal resonator") for rf excitation and signal reception [32].

All animals were examined with T1- and T2-weighted spin-echo pulse sequences and with dynamic contrast-enhanced T1-weighted MRI using the following imaging parameters: for T1-weighted spin-echo MRI: TR = 600 milliseconds; TE = 14 milliseconds, two acquisitions; TA = 3 minutes, 53 seconds; field of view = 60 × 80 mm; matrix = 192 × 256; slice thickness = 1 mm; voxel size = 1.0 × 0.31 × 0.31 mm^3; for T2-weighted fast ("turbo") spin-echo MRI: TR = 4000 milliseconds; TE = 96 milliseconds, one acquisition; echo train length = 7; TA = 1 minute, 49 seconds; field of view = 60 × 80 mm; matrix = 182 × 256; slice thickness = 2 mm; voxel size = 2.0 × 0.33 × 0.31 mm^3. For dynamic contrast-enhanced T1-weighted MRI, we used a spoiled gradient echo sequence fast low-angle shot (FLASH): TR = 100 milliseconds; TE = 6.5 milliseconds; flip angle $\alpha = 90°$, one acquisition; TA = 8 seconds; field of view = 35 × 35 mm; matrix = 64 × 64; slice thickness = 2 mm; voxel size = 2.0 × 0.5 × 0.5 mm^3. During an overall measurement time of 8 minutes, 60 measurements were obtained, with six transversal slices covering the tumor completely.

Analysis of Amplitude and k_{ep} Values

Following Gd-DTPA injection, signal intensity–time curves were recorded. Analysis of the dynamic data was based on the pharmacokinetic two-compartment model of Brix et al. [36]. Compartment 1 is assumed to be the intravascular extracellular space and compartment 2 is the extravascular extracellular space (EES) [24,36]. After infusion of the contrast agent, an exchange of contrast agent between both compartments is assumed, described by the rate constant k_{ep}. k_{ep} is closely related to the downslope of the signal intensity–time curve. Another commonly used functional parameter is the amplitude A—the relative change in signal intensity after the contrast agent injection relative to precontrast values.

Based on this model, the measured data were analyzed. The signal time course was fitted by a Levenberg-Marquard algorithm to the following model equation:

$$\frac{S_{KM}}{S_O}(t) = 1 + \frac{A}{\tau} \times \left\{ \frac{k_{ep} \cdot e^{-k_{el}(t-t_{lag})}}{k_{el}(k_{ep}-k_{el})}(e^{k_{el}t'} - 1) - \frac{\cdot e^{-k_{ep}(t-t_{lag})}}{k_{ep}-k_{el}}(e^{k_{ep}t'} - 1) \right\}$$

with the amplitude:

$$A = D \cdot \frac{V_p}{V_{plasma}} \cdot \frac{k_{pe}}{k_{ep}} \cdot f_1(TR, TE, T_{10}, \alpha, \beta)$$

and

$$t' = \begin{cases} 0 & : t < t_{lag} \\ t - t_{lag} & : t_{lag} < t < \tau + t_{lag} \\ \tau & : t > \tau + t_{lag} \end{cases}$$

The fitting parameters were A, k_{ep}, the renal elimination constant k_{el}, and the time delay of signal enhancement t_{lag}. The amplitude A is proportional to the contrast agent dose D and the fraction of blood volume to voxel volume v_p. It is antiproportional to the whole-body plasma volume V_{plasma} because a higher total plasma volume of the animal results in a higher dilution of the contrast media and thus in a lower amplitude. Furthermore, A depends on sequence and tissue parameters as well as the repetition time TR, the echo time TE, the baseline T_1–time $T_{1,0}$, and the contrast agent relaxivities α and β.

The parameters were calculated pixelwise, color-coded, and overlaid on the morphological MR images.

Additionally, to enable a quantitative comparison of tumor amplitude and k_{ep} of treated and untreated tumors, regions of interest (ROIs) were drawn, using the computer mouse, in

the MR slice with the largest tumor extent for each animal and every examination.

For each tumor, three ROIs were drawn (Figure 1): one including the total tumor, the second placed in the tumor center, and the third at the tumor periphery, as done in previous studies [37,38]. The ROI in the tumor center covered the entire tumor cross-section, but spared the "tumor periphery" (tumor base and tumor convexity), which was defined as a rim approximately 2 mm thick aligned around the entire tumor circumference. The ROI, which intended to represent the tumor periphery, was drawn at the base of the tumor, close to the interface with the apparently nontumorous tissue beneath, but not along the tumor convexity covered by skin. ROIs were placed in a consensus read by three observers (F.K., N.F., and M.L.).

Tumor Volume Measurement

Tumor volume was determined by taking two diameters [length (*a*) and width (*b*)] on the transversal MR image with the largest tumor extent. Assuming the tumor to be an ellipsoid body, the tumor volume *V* was calculated ($V = ab^2\pi/6$).

Histological and Immunofluorescence Examination

Prior to the final MR examination, a line was drawn on the skin of the mice along the largest transversal extent of the tumor, using a pen. This line was then positioned in the middle of the animal resonator under visual control. After excising the tumor, the histologic sections were cut in parallel to this line. For histological diagnosis and assessment of vital tissue and its vascularization, tumors were dissected, covered with "tissue tek" (Sacura, Zoeterwoude, The Netherlands), and frozen in liquid nitrogen vapor. Five-micrometer-thick sections were cut with a Reichert-Jung (Leica-Microsystems, Nussloch, Germany) Frigocut 2700 microtome. Blood vessels and tumor cells were visualized by double immunofluorescence staining using a monoclonal antibody against PECAM (anti–CD 31; PharMingen, San Diego, CA) and a DNA stain with Hoechst (Frankfurt, Germany). Tissue sections were viewed by fluorescence microscopy using an Olympus AX-70 microscope (Olympus America Inc., Melville, NY). Images were captured with an analySIS color view 12 digital camera (Soft Imaging System, Muenster, Germany) and morphometric analyses were performed at × 100 magnification using the analysis SIS (Soft Imaging System) software. Three different fields in the tumor center and at the tumor periphery were examined at × 100 magnification on each section, and the area fraction of the vessel immunofluorescence staining was determined.

Statistics

All statistical evaluations were performed by a professional statistician with the statistical program package SAS for Windows (version 8E; SAS Institute Inc., Cary, NC). Amplitude, k_{ep}, and tumor volumes of each mouse were normalized to the value, which was obtained at the first measurement to minimize preexisting differences between treated and untreated tumors prior to starting the anti–VEGF receptor 2 antibody treatment. Differences in the normalized tumor volume and dynamic parameters of treated and untreated tumors were compared using the two-sided nonparametric Wilcoxon two-sample test. $P < .05$ was determined to be significant. Please note that dynamic data shown in figures and graphs are not normalized in order to improve the transparency of the manuscript.

Results

Monitoring of Tumor Volume

Heterotransplanted SCCs were grown for 2 weeks and had reached a mean volume of 90 mm^3 when treatment with

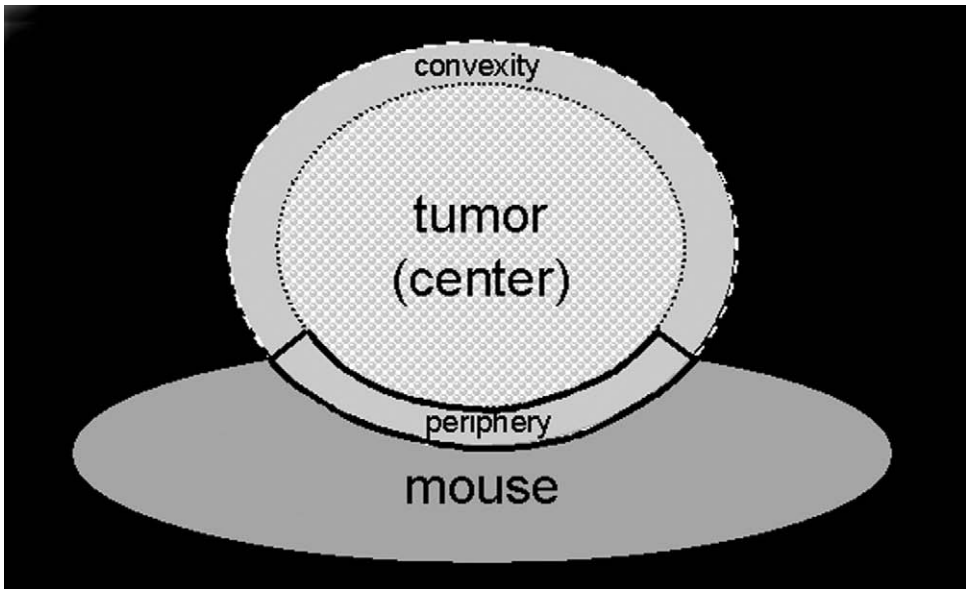

Figure 1. *Sketch illustrating ROI positioning in the tumors for the determination of amplitude and k_{ep} values. One ROI was drawn including the total tumor (dashed line), the second placed in the tumor center (dotted line), and the third at the tumor periphery (continuous line) but sparing the convexity.*

the VEGF receptor 2 blocking antibody, DC 101, started. As early as 4 days after starting the DC 101 treatment, the mean volume (± SD) of treated tumors was lower (190 ± 101 mm^3) compared with untreated ones (437 ± 396 mm^3) (Figure 2). However, due to high interindividual variability, no significant difference was observed compared with the untreated tumors at this date. On day 7, tumor volumes of treated (153 ± 843 mm^3) animals (596 ± 384 mm^3) became significantly smaller ($P = .03$) than those of untreated ones. After 14 days of antibody treatment, the differences were more evident ($P = .02$), with the mean volume of treated tumors of 84 ± 93 mm^3, as compared to 1207 ± 822 mm^3 of controls. At this point of time, one tumor in the treatment group was even no longer detectable by MRI.

Noninvasive MR Monitoring of Tumor Volume and Tumor Perfusion

MR parameter maps of amplitude and k_{ep} were established to noninvasively visualize changes in both tumor volume and vascularization (Figure 3). During follow-up, the amplitude decreased in both treated and untreated tumors, which was most pronounced in tumor centers. However, the decrease of amplitude was observed much earlier in treated tumors than in the untreated controls (Figure 3). After 2 days of treatment, spots in central tumor parts started to display very low amplitudes. Two days later, although tumor volumes still remained unchanged, the whole center of the treated tumor homogeneously showed very low amplitudes (Figure 3). Then, at 7 and 14 days after starting the antiangiogenic treatment, the volumes of the treated tumors markedly decreased. In contrast, untreated tumors continuously increased in volume. As a general impression, areas without increase of signal intensity (no measurable amplitude and k_{ep} values) developed to a much lower degree, and later than in treated animals. After 4, 7, and 14 days, all untreated tumors showed a mixed pattern of large areas with high and low amplitudes and k_{ep}.

Comparison of MR Monitoring and Histological Parameters

To validate MR parameter maps, they were compared with corresponding histological sections stained for tumor vessels by immunofluorescence. Amplitude/k_{ep} parameter maps of tumors at days 1, 2, and 4 after the start of the VEGF receptor antibody treatment are shown with the corresponding immunofluorescence images (Figure 4). All histologically apparent structures above 2 mm diameter, such as necrotic and solid tumor areas, respectively, were clearly identified with amplitude/k_{ep} parameter maps in all tumors analyzed.

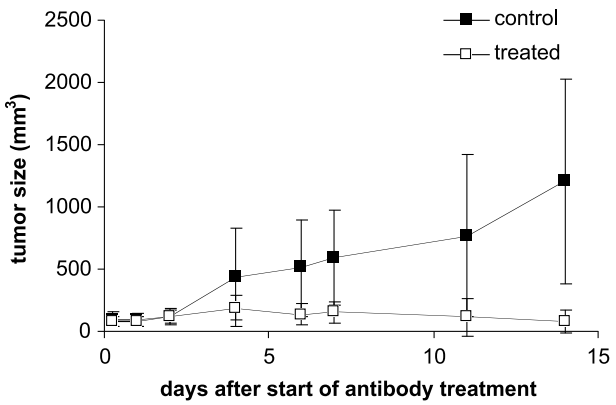

Figure 2. *Mean tumor volumes of treated and untreated tumors (mean ± SD). Treated tumors slowed growth and showed significantly lower tumor volumes, whereas untreated tumors continuously increased volume.*

The considerable decrease in amplitude levels in the center of treated tumors that was observed during the first week was mirrored by necrotic areas in the tumor center and a large decrease in vessel density in immunofluorescence images (Figure 5). After 7 days of treatment, only a small rim with solid tumor tissue and persistent vessels remained (not shown). After 2 weeks of treatment, when the volume of the treated tumors had markedly decreased, the necrotic centers were abolished and the remaining peripheral tumor parts, which continued to display high amplitudes, showed large vessels at the tumor base and in the overlying skin.

Quantitative Evaluation of Tumor Perfusion

Amplitudes and k_{ep} were measured in ROIs covering the total tumor, tumor center, and tumor periphery separately (Figures 6 and 7). The behavior of the amplitudes of treated and untreated tumors differed significantly, with respect to the total tumor ROIs and the ROIs of the tumor center. Amplitudes of the tumor periphery revealed no significant difference throughout the experiment (Figures 6 and 7).

For the total tumor and tumor center, the differences in amplitude between treated and untreated tumors were most significant 4 days after starting antibody treatment. Although the tumor volume showed no significant changes, the amplitudes in treated tumors decreased by 64% in the total tumor ROIs and by 84% in ROIs of the tumor center, whereas amplitudes in untreated tumors decreased by only 30% for the total tumor and by 40% for the tumor center ($P = .02$) (Figure 6). After 7 days of therapy, amplitudes of total tumor and tumor center rose again in the four treated tumors, which were examined successfully at the last examination date, reaching a mean amplitude of 39% and 72%, respectively, above control (Figure 7). This increase was paralleled by a significant decrease in tumor volume in the treated tumors. Simultaneously, untreated tumors increased in volume and started to display necrotic areas.

In contrast, the exchange rate constant k_{ep}, which is a compound parameter highly influenced by vessel permeability, did not change significantly in treated and untreated tumors during follow-up, remaining comparable between both groups (Figure 7).

In agreement with the change of MR amplitudes, histologically determined microvessel density in the tumor centers of untreated tumors continuously decreased during follow-up. Furthermore, microvessel density in the centers of treated tumors decreased earlier and to a higher degree than in the untreated ones. In concordance with the change of amplitudes in tumor centers from 7 to 14 days, microvessel density tended to become higher in treated than in untreated tumors, thereby validating noninvasive MRI as a suitable

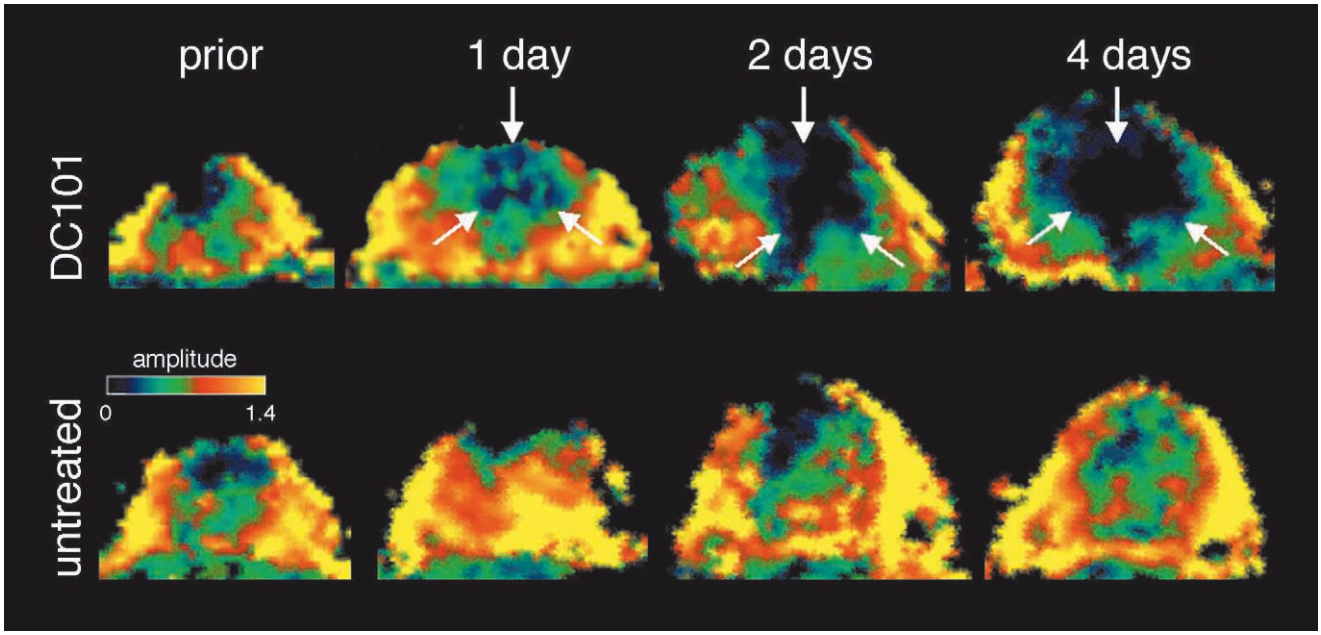

Figure 3. *Follow-up of color-coded amplitude parameter maps of a treated and an untreated tumor, which was examined prior (0) and 1, 2, and 4 days after start of the antibody treatment. Two days after start of antibody treatment, spots occurred in the tumor center, which did not show any contrast enhancement (arrows). After 4 days, no enhancement was found and thus no amplitudes could be calculated in central tumor areas anymore (arrows). In contrast, the untreated tumor increased volume continuously. Also in untreated tumors, a decrease on central amplitude values was observed was but less pronounced and started at later time points. During these 4 days of treatment, no significant differences were observed in tumor volume between the treated and the untreated tumors.*

method for monitoring tumor vascularization under antiangiogenic therapy (Figure 8*A*). In contrast, microvessel density in the tumor periphery did not change markedly during the examination period (Figure 8*B*).

Discussion

Angiogenic switch is a key event in tumor progression to a malignant, invasive, and ultimately metastasizing tumor, making angiogenesis one of the most promising targets for the novel concepts of cancer therapy. The efficacy of antiangiogenic treatments for tumor regression and suppression of metastases has been demonstrated in animal models and is continuously being improved [3,10,12]. However, the monitoring of the kinetics of therapeutic response has been proven difficult. It was predominantly the use of histological methods needing extensive experimental protocols with a large number of animals that has been successful so far. The development of functional noninvasive monitoring methods that can be performed without the need for high-field MR scanners is therefore an urgent necessity.

In the work presented here, T1-weighted DCE MRI utilizing a 1.5-T whole-body MR scanner and the parameterization with the two-compartment model of Brix et al. were used to monitor the kinetics of changes in tumor vascularization in nude mice treated with an anti–VEGF receptor 2 antibody. The two-compartment model describes extravasation and rediffusion of contrast agent between an intravascular and an extravascular extracellular compartment. Although the simple design may not consider the vascular tumor pathology in all regards (some amounts of contrast media may, for example, be trapped in necrotic regions or be eliminated by lymphatic vessels), it has proven reliable in various experimental and clinical studies [16,23,25–27]. Using a simple model is of critical importance when small animals are examined in a clinical scanner with a considerably low signal-to-noise ratio.

One key parameter used for monitoring is the amplitude, which reflects the increase in signal intensity relative to precontrast values. It is assumed that the intravascular fraction of contrast agent hardly contributes to the change in signal intensity. Only the contrast agent that exits the vessels and enters the interstitial space will be present in amounts sufficient to cause relevant signal enhancement. The more blood is present inside the tissue volume, the more contrast agent will be delivered to the interstitial space, and the higher will be the amplitude [23,37]. Indeed, it was shown previously that the amplitude correlates significantly with microvessel density in HaCaT-ras heterotransplant tumors [38]. The exchange rate constant k_{ep} is a compound parameter, which is closely related to the slope of the signal–intensity time curve and is considered to largely reflect vessel permeability but also the vessel surface area and perfusion. Which of these factors most determines k_{ep} will depend on which process is the limiting one for the substance exchange between the two compartments under given conditions. Unfortunately, the validation of k_{ep} as parameter of vessel permeability [23] is still missing due to the lack of standardization with direct measurements. Whenever the intention is to measure blood flow or volume, it is the most serious limitation of the two-compartment model that the estimations are based on indirect measurements of the contrast agent's entry into the extravascular space and not, as in fast dynamic MR measurements (e.g., T2*-DCE MRI or

arterial spin labeling techniques), on the inflow of blood itself into the tissue. As a precondition for using the two-compartment model, the contrast agent has to be homogeneously distributed in the whole circulation, which is usually guaranteed by a sufficiently high blood flow. Whenever the blood flow is very low (e.g., in malignant tumors with irregular vascularization), perfusion will become the limiting process, and the exchange rate constant k_{ep} will be more influenced by perfusion than by permeability. To reach a homogeneous distribution of the contrast agent, in most previous clinical studies, contrast agent was injected as an infusion, not as bolus as in our study. The reason for us to use a bolus injection was that 100 μl of contrast agent can hardly be given as an infusion without a suitable injection pump, which was not available in our case. However, circulation time of the total blood volume in mice is only 8 seconds and thus about 10 times faster than in humans [39]. Therefore, it can be assumed that in mice, the contrast agent is homogeneously distributed within a few seconds, and the precondition for using the Brix et al. model is fulfilled. In order to enlarge the sensitivity of the method, the contrast agent dose was optimized such that amplitude was comparable to those of human studies. Therefore, in our study, four times the dose of Gd-DTPA as used in human studies was applied. Although we do not know the local concentration of the contrast agent in our presented model, inside the tumor, we did not observe a T2 effect after contrast agent injection.

By comparing tumor volumes of treated and untreated tumors, we could clearly demonstrate that tumors treated with the inhibitory VEGF receptor 2 antibody, DC101, grew much slower than controls or were even reduced in volume. Although a prolonged growth was observed during the first week, the volume reduction of treated tumors became most prominent during the second week of treatment. In line with previous results on colorectal cancers in patients treated with an inhibitor of the VEGF receptor [40], effects on tumor

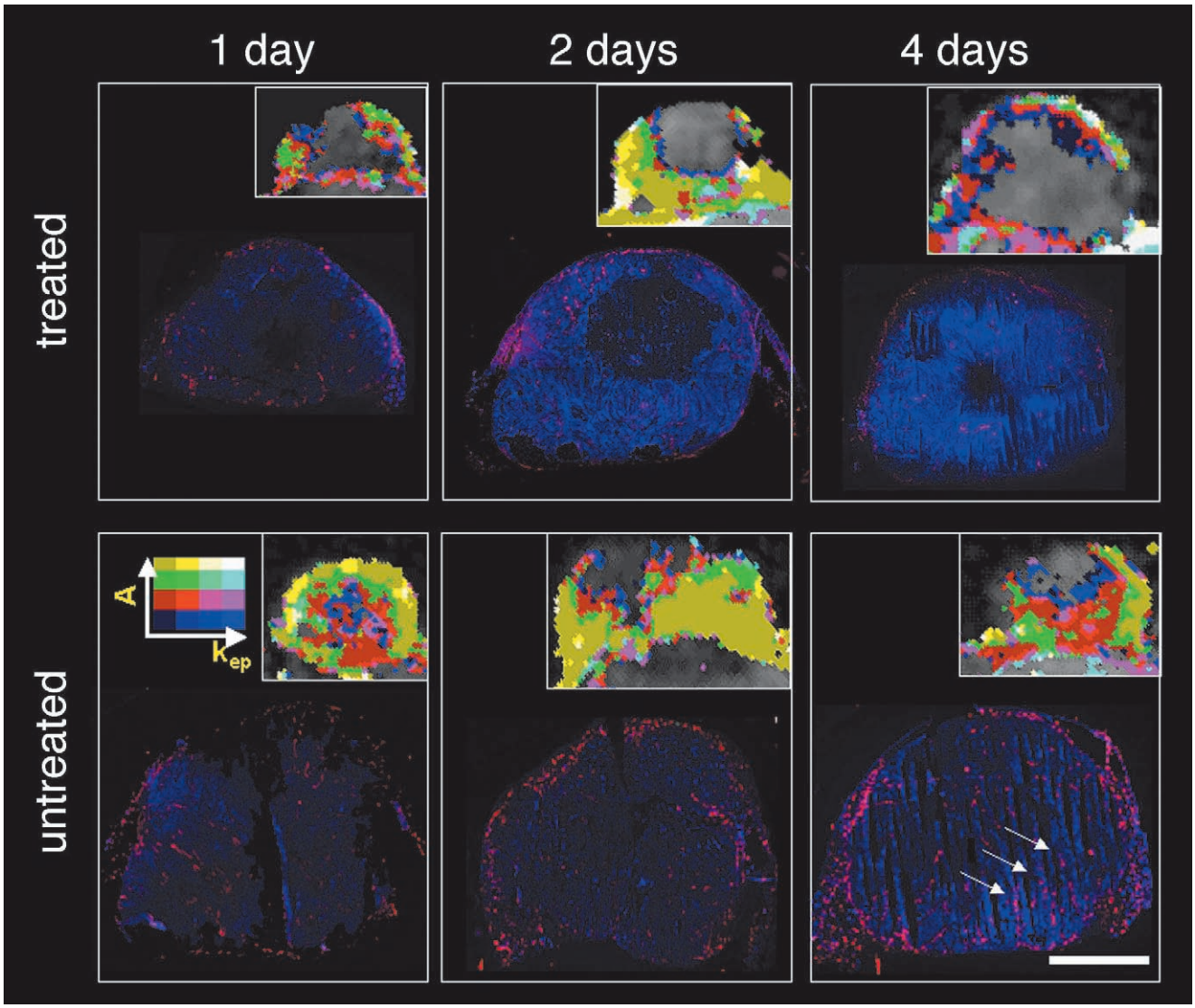

Figure 4. *Color-coded parameter maps of amplitude/k_{ep} and the corresponding immunofluorescence images (bottom row) of treated and untreated tumors are shown after 1, 2, and 4 days of VEGF receptor antibody treatment. Vessels were stained with a CD31 antibody (red). Tumor cells were visualized with Hoechst DNA stain (blue). The treatment with the VEGF receptor antibody caused a decrease on amplitudes and a loss of tumor vessels, which was accentuated in tumor centers. Bar = 5 mm.*

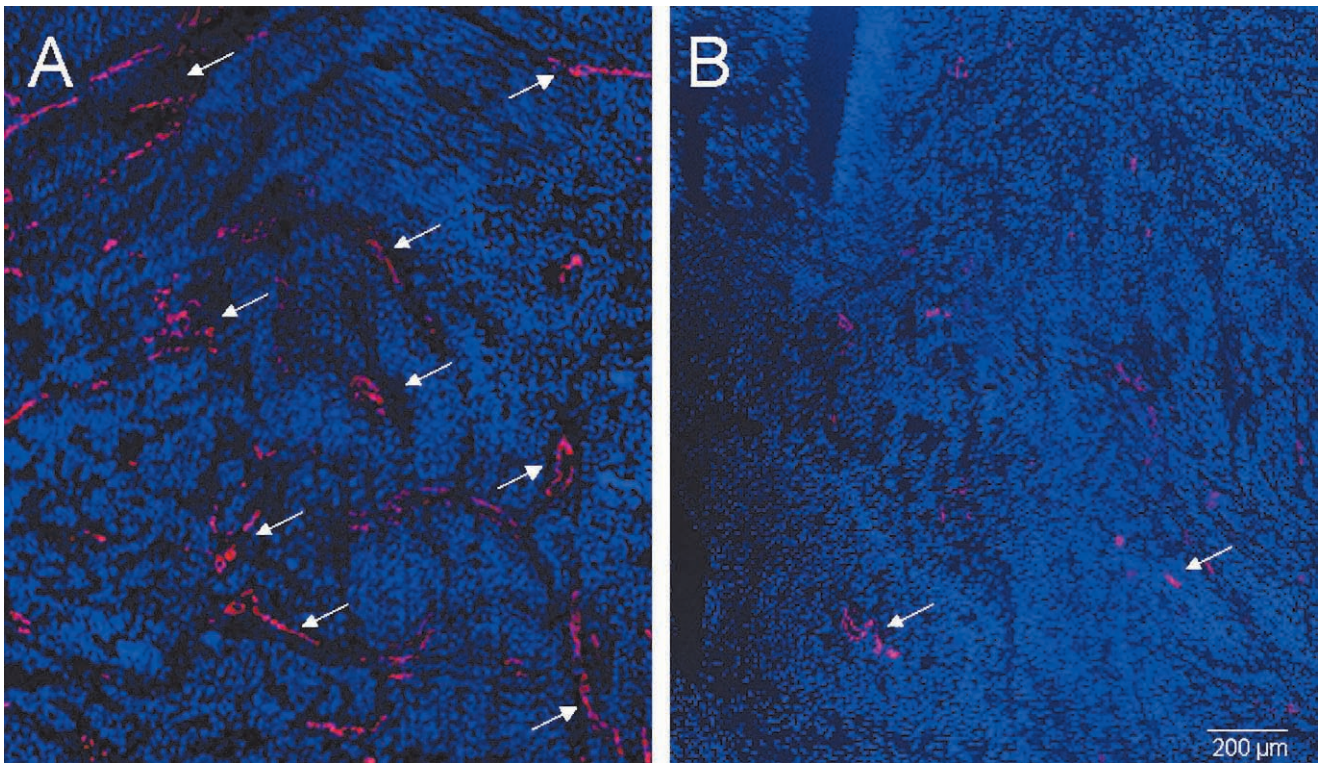

Figure 5. *Double immunofluorescence images recorded in the centers of an untreated (A) and a 4-day–treated HaCaT-ras tumor (B). Vessels were stained with a CD31 antibody (red). Tumor cells were visualized with Hoechst DNA stain (blue). Compared with the control, the treated tumor shows a marked decrease in vessel density (larger vessels are labeled with arrows). Bar = 200 µm.*

vascularization of the SCC xenografts preceded volume reduction of tumors and were reflected by a decrease in amplitude levels and microvessel density already within two treatments after the first. During the second week of treatment, tumor amplitudes rose again in treated animals, reaching higher levels than in controls at 14 days posttreatment. During this interval, the treated tumors continued to decrease in volume. There are several aspects that explain this seemingly paradoxical result. The DC101 treatment affects mainly the small immature vessels inside the tumors that represent the major contributors to tumor nutrition. Mature vessels (i.e., vessels with pericytes) or vessel threads might be less influenced because they are less dependent on angiogenic stimulation. The decrease of microvascularization will have a strong effect on the tumor cells, which become necrotic and then are degraded, causing tumor shrinkage. Due to the persistence of larger mature vessels and the fact that higher vascularized areas of the tumor periphery draw nearer due to the loss of tumor cell mass, the reduction of intravascular volume and thus the amplitude might not have kept pace with tumor shrinkage. At the same time, the delineation of treated tumors, which had reached very small volumes, is more difficult and the ROIs may have not exclusively contained tumor tissues but also included large subcutaneous vessels giving a high amplitude. These mature vessels are not sensitive to the VEGF receptor blockade, leaving them unaltered during treatment. Furthermore, although treated tumors showed good perfusion in the entire tumor after 2 weeks, continuously decreasing amplitude values were found in untreated tumors during the whole examination period. This is most likely due to the development of hypoperfused central necroses during the later stages of tumor growth that were rather dominant in the histological sections [37]. As a consequence, we see a significant decrease in amplitude in the tumor center, whereas it was considerably less pronounced in the tumor periphery. The results are also in line with those of intermittent ultrasound, where a decrease in tumor perfusion and blood volume was observed during the first week, followed by an increase within the second week after starting VEGF receptor 2 antibody treatment [41].

No significant differences between treated and untreated animals were observed for k_{ep}, although VEGF highly increases vessel permeability and vessel diameter, and thus the vessel surface area [15]. As a consequence of blocking VEGF effects, a decrease of vessel permeability was expected, which was described in previous studies using DCE MRI for heterotransplanted tumor models of brain [42], breast [43], and colorectal cancers of patients [39]. Considering the fact that k_{ep} is influenced by both vessel permeability and vessel surface area, k_{ep} should decrease if both a reduction of vessel surface area (vasoconstriction) and permeability occur. There are two explanations for the observed unchanged k_{ep} during follow-up in this study: the early treatment effects may have unexpectedly increased vessel permeability by affecting the integrity of the vessel wall and the resulting increase of k_{ep} may then be balanced by a reduction of the vessel surface area (or blood flow, in case

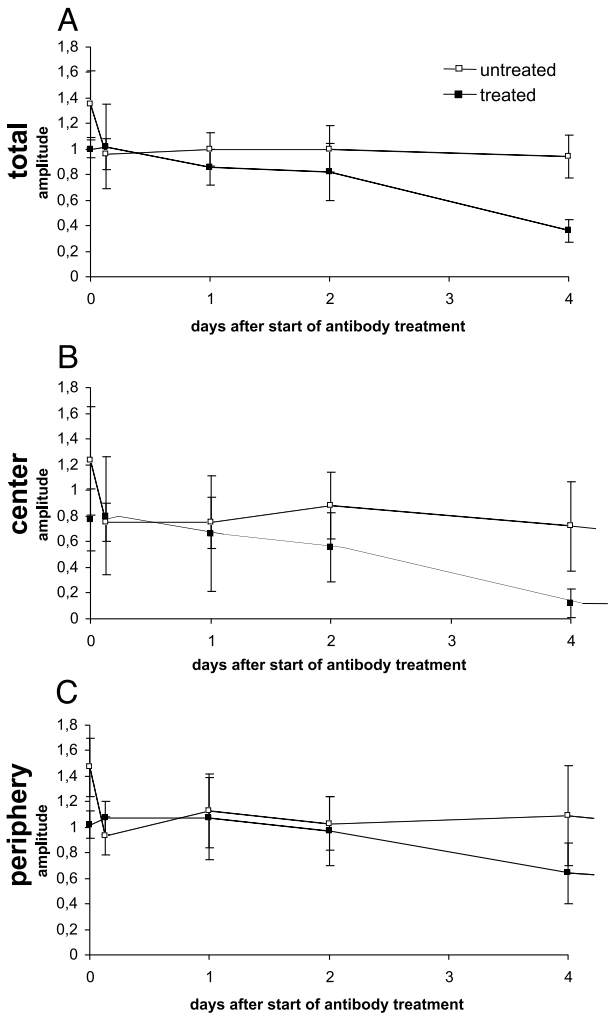

Figure 6. *Amplitudes in treated and untreated tumors measured in ROIs of the total tumor (A), tumor center (B), and tumor periphery (C) during the initial 4 days of treatment. Data are given as mean ± SD.*

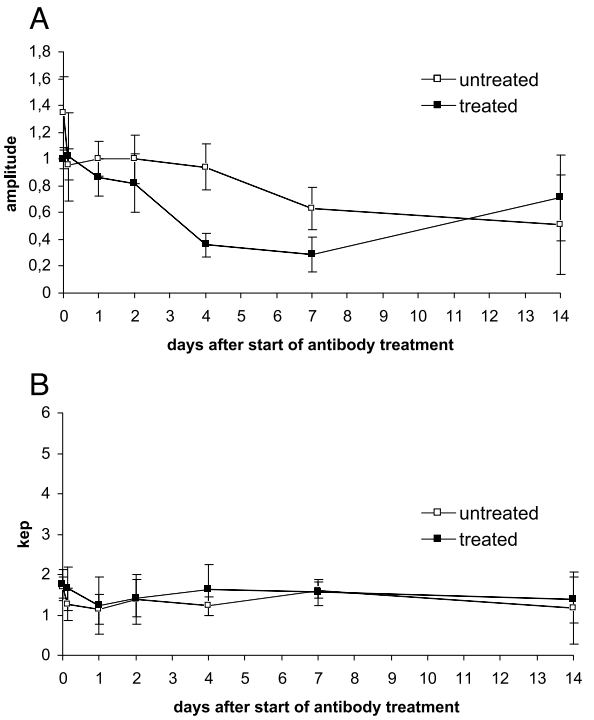

Figure 7. *Amplitudes (A) and k_{ep} (B) of treated and untreated tumors measured in ROIs of total tumors during the 14-day follow-up. Data are given as mean ± SD. Amplitudes of treated tumors rapidly decrease during the initial 4 days of treatment, but then rise again and are higher than in the controls after 14 days. Amplitudes of untreated tumors decrease continuously. In contrast, k_{ep} shows stable values over the whole examination period and no significant differences are observed between treated and untreated tumors.*

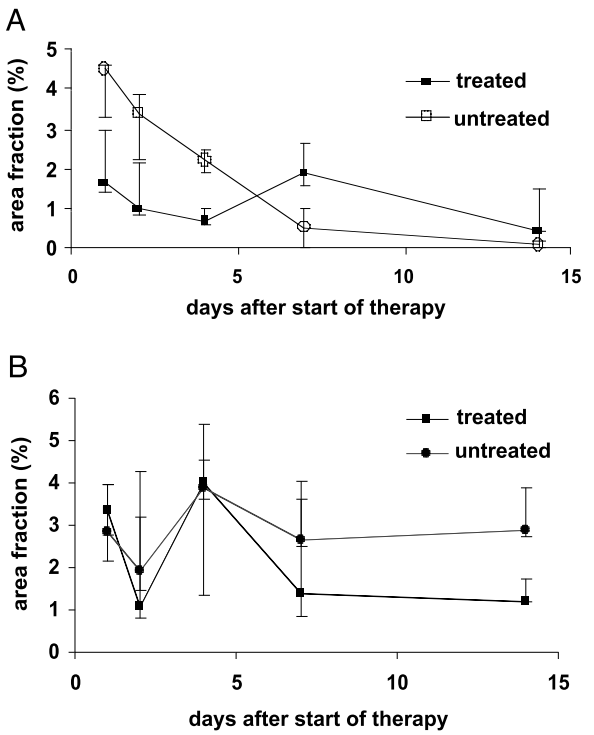

Figure 8. *Microvessel densities (area fraction) measured in the tumor center (A) and tumor periphery (B). At each time point, one treated and one untreated tumor were examined. For each tumor in the center and the periphery, microvessel density was determined in three different fields. The median value and the higher and lower values (error bars) are given.*

this model is limited by perfusion), resulting in an unchanged k_{ep}. The second possibility is that the integrity of the vascular wall is not affected by the DC101 treatment at all and thus k_{ep} remains unchanged. Due to higher sensitivity for larger defects and pores of the vessel wall, which are typical marks of immature neoplastic vascularization, macromolecular contrast agents such as Gd-DTPA albumin [32] or Gd-labeled graft polymers may be more suitable to work out specific effects on vessel permeability [44,45]. However, most of these contrast agents show a slow but long accumulation in tumors, which limits their usability for follow-up studies with close time intervals.

Summarizing our results, we have shown the high therapeutic potential of the DC101 antibody as antiangiogenic treatment of human SCCs in nude mice. Using T1w DCE MRI and the two-compartment model, early therapeutic response, which preceded volume reduction of tumors, was observed as early as 2 days after the first antibody treatment. Maximum difference in tumor vascularization between treated tumors and controls was reached after 4 days. However, at later therapy stages in collapsing

tumors, there is a risk of misinterpretation caused by the tighter grouping of vessels in the tumors, which induces an increase of dynamic parameters.

Acknowledgement

We thank Ivan Zuna for the statistical evaluation of our data and the critical reading of the manuscript.

References

[1] Carmeliet P and Jain RK (2000). Angiogenesis in cancer and other diseases. *Nature* **407,** 249–257.

[2] Folkman J (2001). Angiogenesis-dependent diseases. *Semin Oncol* **28,** 536–542.

[3] Folkman J (1995). Angiogenesis in cancer, vascular, rheumatoid and other disease. *Nat Med* **1,** 27–31.

[4] Fox SB, Gasparini G, and Harris AL (2001). Angiogenesis: pathological, prognostic, and growth-factor pathways and their link to trial design and anticancer drugs. *Lancet Oncol* **2,** 278–289.

[5] Scappaticci FA (2002). Mechanisms and future directions for angiogenesis-based cancer therapies. *J Clin Oncol* **20,** 3906–3927.

[6] Brekken RA, Overholser JP, Stastny VA, Waltenberger J, Minna JD, and Thorpe PE (2000). Selective inhibition of vascular endothelial growth factor (VEGF) receptor 2 (KDR/Flk-1) activity by a monoclonal anti-VEGF antibody blocks tumor growth in mice. *Cancer Res* **60,** 5117–5124.

[7] Kuba K, Matsumoto K, Date K, Shimura H, Tanaka M, and Nakamura T (2000). HGF/NK4, a four-kringle antagonist of hepatocyte growth factor, is an angiogenesis inhibitor that suppresses tumor growth and metastasis in mice. *Cancer Res* **60,** 6737–6743.

[8] Klement G, Baruchel S, Rak J, Man S, Clark K, Hicklin DJ, Bohlen P, and Kerbel RS (2000). Continuous low-dose therapy with vinblastine and VEGF receptor-2 antibody induces sustained tumor regression without overt toxicity. *J Clin Invest* **105,** 15–24.

[9] Gasparini G (2001). Metronomic scheduling: the future of chemotherapy? *Lancet Oncol* **2,** 733–740.

[10] Jain RK (2001). Normalizing tumor vasculature with anti–angiogenic therapy: a new paradigm for combination therapy. *Nat Med* **7,** 987–989.

[11] Klement G, Baruchel S, Rak J, Man S, Clark K, Hicklin D, Bohlen P, and Kerbel S (2000). Continuous low-dose therapy with vinblastine and VEGF receptor-2 antibody induces sustained tumor regression without overt toxicity. *Clin Invest* **105,** R15–R24.

[12] Kerbel RS (2000). Tumor angiogenesis: past, present and the near future. *Carcinogenesis* **21,** 505–515.

[13] Holash J, Maisonpierre PC, Compton D, Boland P, Alexander CR, Zagzag D, Yancopoulos GD, and Wiegand SJ (1999). Vessel cooption, regression, and growth in tumors mediated by angiopoeitins and VEGF. *Science* **284,** 1994–1998.

[14] Thomas KA (1996). Vascular endothelial growth factor, a potent and selective angiogenic agent. *J Biol Chem* **271,** 603–606.

[15] Neufeld G, Cohen T, Gengrinovitch S, and Poltorak Z (1999). Vascular endothelial growth factor (VEGF) and its receptors. *FASEB J* **13,** 9–22.

[16] Knopp MV, Giesel FL, Marcos H, von Tengg-Kobligk H, and Choyke P (2001). Dynamic contrast-enhanced magnetic resonance imaging in oncology. *Top Magn Reson Imaging* **12,** 301–308.

[17] Padhani R and Husband JE (2001). Dynamic contrast-enhanced MRI studies in oncology with an emphasis on quantification, validation and human studies. *Clin Radiol* **56,** 607–620.

[18] Lyng H, Dahle GA, Kaalhus O, Skretting A, and Rofstad EK (1998). Measurement of perfusion rate in human melanoma xenographs by contrast enhanced magnetic resonance imaging. *Magn Reson Med* **40,** 89–98.

[19] Abramovitch R, Dafni H, Neeman M, Nagler A, and Pines M (1999). Inhibition of neovascularization and tumor growth, and facilitation of wound repair, by halofuginone, an inhibitor of collagen type I synthesis. *Neoplasia* **1,** 321–329.

[20] Neeman M, Provenzale JM, and Dewhirst MW (2001). Magnetic resonance imaging applications in the evaluation of tumor angiogenesis. *Semin Radiat Oncol* **11,** 70–82.

[21] Bhujwalla ZM, Artemov D, Natarajan K, Ackerstaff E, and Solaiyappan M (2001). Vascular differences detected by MRI for metastatic *versus* nonmetastatic breast and prostate cancer xenografts. *Neoplasia* **3,** 143–153.

[22] Tropres I, Grimault S, Vaeth A, Grillon E, Julien C, Payen JF, Lamalle L, and Decorps M (2001). Vessel size imaging. *Magn Reson Med* **45,** 397–408.

[23] Hoffmann U, Brix G, Knopp MV, Hess T, and Lorenz WJ (1995). Pharmacokinetic mapping of the breast: a new method for dynamic MR mammography. *Magn Reson Med* **33,** 506–514.

[24] Port RE, Knopp MV, Hoffmann U, Milker-Zabel S, and Brix G (1999). Multicompartment analysis of gadolinium chelate kinetics: blood–tissue exchange in mammary tumors as monitored by dynamic MR imaging. *J Magn Reson Imaging* **10,** 233–241.

[25] Hawighorst H, Weikel W, Knapstein PG, Knopp MV, Zuna I, Schonberg SO, Vaupel P, and van Kaick G (1998). Angiogenic activity of cervical carcinoma: assessment by functional magnetic resonance imaging-based parameters and a histomorphological approach in correlation with disease outcome. *Clin Cancer Res* **4,** 2305–2312.

[26] Hawighorst H, Knapstein PG, Knopp MV, Vaupel P, and van Kaick G (1999). Cervical carcinoma: standard and pharmacokinetic analysis of time–intensity curves for assessment of tumor angiogenesis and patient survival. *Magma* **8,** 55–62.

[27] Moehler TM, Hawighorst H, Neben K, Egerer G, Hillengass J, Max R, Benner A, Ho AD, and van Kaick G (2001). Bone marrow microcirculation analysis in multiple myeloma by contrast-enhanced dynamic magnetic resonance imaging. *Int J Cancer* **93,** 862–868.

[28] Abramovitch R, Meir G, and Neeman M (1995). Neovascularization induced growth of implanted C6 glioma multicellular spheroids: magnetic resonance microimaging. *Cancer Res* **55,** 1956–1962.

[29] Weissleder R, Bogdanov A, Tung CH, and Weinmann HJ (2001). Size optimization of synthetic graft copolymers for *in vivo* angiogenesis imaging. *Bioconjug Chem* **12,** 213–219.

[30] Turetschek K, Huber S, Floyd E, Helbich T, Roberts TP, Shames DM, Tarlo KS, Wendland MF, and Brasch RC (2001). MR imaging characterization of microvessels in experimental breast tumors by using a particulate contrast agent with histopathologic correlation. *Radiology* **218,** 562–569.

[31] Brasch R, Pham C, Shames D, Roberts T, van Dijke K, van Bruggen N, Mann J, Ostrowitzki S, and Melnyk O (1997). Assessing tumor angiogenesis using macromolecular MR imaging contrast media. *Magn Reson Imaging* **7,** 68–74.

[32] Kiessling F, Fink C, Hansen M, Bock M, Sinn H, Schrenk HH, Krix M, Egelhof T, Fusenig NE, and Delorme S (2002). Magnetic Resonance Imaging of nude mice with heterotransplanted high-grade squamous cell carcinomas (SCC): use of a low loaded, covalently bound Gd-HSA conjugate as contrast agent with high tumor affinity. *J Invest Radiol* **37,** 193–198.

[33] Skobe M, Rockwell P, Goldstein N, Vosseler S, and Fusenig NE (1997). Halting angiogenesis suppresses carcinoma cell invasion. *Nat Med* **3,** 1222–1227.

[34] Fusenig NE and Boukamp P (1998). Multiple stages and genetic alterations in immortalization, malignant transformation, and tumor progression of human skin keratinocytes. *J Mol Carcinog* **23,** 144–158.

[35] Mueller M, Peter W, Mappes M, Huelsen A, Steinbauer H, Boukamp P, Vaccariello M, Garlick J, and Fusenig NE (2001). Tumor progression of skin carcinoma cells *in vivo* promoted by clonal selection, mutagenesis, and autocrine growth regulation by granulocyte colony-stimulating factor and granulocyte–macrophage colony-stimulating factor. *Am J Pathol* **159,** 1567–1579.

[36] Brix G, Semmler W, Port R, Schad LR, Layer G, and Lorenz WJ (1991). Pharmacokinetic parameters in CNS Gd-DTPA enhanced MR imaging. *J Comput-Assist Tomogr* **15,** 621–628.

[37] Kiessling F, Heilmann M, Vosseler S, Lichy M, Krix M, Fink C, Kiessling I, Steinbauer H, Schad L, Fusenig NE, and Delorme S (2003). T1-dynamic monitoring of vascularization in human carcinoma heterotransplants by magnetic resonance imaging. *Int J Cancer* **104,** 113–120.

[38] Kiessling F, Krix M, Heilmann M, Vosseler S, Lichy M, Fink C, Farhan N, Kleinschmidt K, Schad L, Fusenig NE, and Delorme S (2003). Comparing dynamic parameters of tumor vascularisation in nude mice revealed by MRI and intermittent power Doppler sonography. *Invest Radiol* **38,** 516–524.

[39] Kaplan HM, Brewer NR, and Blair WH (1983). The Mouse in Biomedical Research. In Foster, HL, Small, JD, Fox, JG (Eds.), p. 251 Academic Press, New York.

[40] Morgan B, Thomas AL, Drevs J, Hennig J, Buchert M, Jivan A, Horsfield MA, Mross K, Ball HA, Lee L, Mietlowski W, Fuxuis S, Unger C, O'Byrne K, Henry A, Cherryman GR, Laurent D, Dugan M,

Brasch RC, and Steward WP (2003). Dynamic contrast-enhanced magnetic resonance imaging as a biomarker for the pharmacological response of PTK787/ZK 222584, an inhibitor of the vascular endothelial growth factor receptor tyrosine kinases, in patients with advanced colorectal cancer and liver metastases: results from two phase I studies. *J Clin Oncol* **21,** 3955–3964.

[41] Krix M, Kiessling F, Vosseler S, Farhan N, Bohlen P, Fusenig NE, and Delorme S (2003). Monitoring tumor perfusion during antiangiogenic therapy with intermittent bolus-contrast power Doppler sonography. *Cancer Res* (in press).

[42] Gossmann A, Helbich TH, Kuriyama N, Ostrowitzki S, Roberts TPL, Shames DM, van Bruggen N, Wendland MF, Israel MA, and Brasch RC (2002). Dynamic contrast-enhanced magnetic resonance imaging as a surrogate marker of tumor response to anti–angiogenic therapy in a xenograft model of glioblastoma multiforme. *J Magn Reson Imaging* **15,** 233–240.

[43] Brasch R, Pham C, Shames D, Roberts T, van Dijke K, van Bruggen N, Mann J, Ostrowitzki S, and Melnyk O (1997). Assessing tumor angiogenesis using macromolecular MR imaging contrast media. *J Magn Reson Imaging* **7,** 68–74.

[44] Bogdanov AA, Lewin M, and Weissleder R (1999). Approaches and agents for imaging the vascular system. *Adv Drug Deliv Rev* **37,** 279–293.

[45] Gossmann A, Okuhata Y, Shames DM, Helbich TH, Roberts TPL, Wendland MF, Huber S, and Brasch RC (1999). Prostate cancer tumor grade differentiation with dynamic contrast-enhanced MR imaging in the rat: comparison of macromolecular and small-molecular contrast media—preliminary experience. *Radiology* **213,** 265–272.